White matter characterization in regions of edema surrounding meningioma brain tumor using diffusion MRI: A comparative study of DTI and NODDI.

Sasha Hakhu, Ph.D.[1]; Parvathy Hareesh[1]; Andrew Hooyman, Ph.D.[1]; Jennapher Lingo VanGilder, Ph.D.[1]; Jason Yalim, Ph.D. [2]; Leslie Baxter, Ph.D. [3]; Leland Hu, M.D.[3]; Yuxiang Zhou, Ph.D.[3]; Kurt Schilling, Ph.D.[4]; Scott C. Beeman, Ph.D.[1]

[1]School of Biological and Health Systems Engineering, Arizona State University, Tempe, AZ; [2]Computational Research Accelerator, Arizona State University, Tempe, AZ; [3]Mayo Clinic, Phoenix, AZ; [4]Vanderbilt University, Nashville, TN

Corresponding author: Scott Beeman, Ph.D.; scott.beeman@asu.edu; 550 E Orange St., Tempe, AZ 85287.

Abstract

White matter (WM) tract detection is critical in presurgical planning of tumor resection; however, standard-of-care diffusion tensor imaging (DTI) often fails to characterize white matter tracts through regions of edema. This is because the presence of edema has the effect of increasing the isotropic volume fraction within a voxel and thus marginalizing the anisotropic volume fraction associated with white matter presence and directionality. More recent biophysical models of diffusion, such as neurite orientation dispersion and density imaging (NODDI), account for isotropic and anisotropic volume fractions within voxels by compartmentalizing the diffusion signal based on an assumed tissue microenvironment, e.g., "free water" (cerebrospinal fluid (CSF), interstitial fluid (ISF), edema), "intra-neurite", and "extra-neurite" tissue, as a sphere, stick, and tensor, respectively. We hypothesize that a low fractional anisotropy (FA), low orientation dispersion index (ODI) value and high fractional isotropic volume (FISO) would be observed in white matter regions containing edema but a high FA, low ODI value and low FISO would be observed in healthy-appearing contralateral white matter. In our study, we test this hypothesis using multi-shell diffusion MRI data collected from patients bearing meningioma brains tumors. Brains bearing meningioma tumors are selected in this study as meningiomas rarely invade the brain parenchyma and we can thus assume that our analyses of edematous regions are not confounded by infiltrating tumor cells. Here, we show that NODDI-based characterization of white matter is more sensitive than that of standard-of-care DTI through regions of edema. Future studies will focus on implementation of biophysical model-based tractography in cases of glioma and translation of biophysical model-based tractography to the operating room.

1. Introduction

Preoperative surgical mapping of brain structures is performed to improve the accuracy of neurosurgery and reduce the risk of complications. Accurate detection of white matter (WM) structures in peritumoral regions remains challenging because conventional magnetic resonance imaging (MRI) techniques, such as T1-weighted (T1-w), T2-weighted (T2-w), and diffusion tensor imaging (DTI), often fail to delineate WM when present in regions of edema, a characteristic accumulation of interstitial fluid surrounding the tumor [1], [2], [3], [4], [5], [6]. At a fundamental level, this is due to the lack of relaxation-driven signal contrast in these regions in the case of T1- and T2-weighted imaging or a failure to separate isotropic from anisotropic diffusion within a voxel in the case of DTI. In patients with brain tumors, characterizing white matter (WM) microstructure (i.e, ensuring their visibility in images) is especially critical in regions affected by edema. Conventional imaging techniques like T1-weighted and T2-FLAIR (fluid attenuated inversion recovery) scans do not reveal the underlying microstructural changes caused by edema. In tumor-infiltrated cases, basic anatomical knowledge does not apply, as mass effect [7], [8], [9] and tumor-induced tissue changes complicate visual assessments. To address this, we focus on a control group of meningioma patients, where WM tracts remain uncontaminated by tumor cells. Advanced diffusion models offer enhanced microstructural insight that is particularly relevant for clinical scenarios such as pre-surgical planning, where understanding the extent of tissue disruption is essential for minimizing damage to healthy WM tracts. Additionally, besides merely improving visibility of these tracts in images, we are focused on providing an index that is specific to neurites and unconfounded by other conditions.

Diffusion MRI (dMRI) is sensitive to the displacement of water molecules within the constraints of the complex tissue microenvironment and, when dMRI data are rationally

acquired, one can use dMRI to make quantitative inference of tissue microstructure (e.g., WM tract directionality, axon and dendrite density, and orientation complexity) through tensor calculation and/or biophysical modeling of the dMRI data [7]–[12]. DTI, which is a common and simple tensor calculation-based implementation of diffusion MRI [16], [17], yields the so-called mean diffusivity (MD) and fractional anisotropy (FA) metrics, of which we will principally focus on the FA metric herein. FA is scaled from 0 to 1 and is used to quantify the degree of directionality of proton displacement in the tissue. In white matter, the diffusion-driven displacement of water is typically anisotropic (greater in one direction than the others) due to the coherent orientation of white matter bundles and hence is expected to have a higher FA value. This mechanism forms the foundation of most diffusion-based study of white matter in brain. However, the utility of DTI, which is unable to compartmentalize isotropic from anisotropic diffusion components within a single voxel, can fail to characterize white matter in pathologies that involve significant edema in WM (e.g., brain tumor). In this case, edema has the effect of increasing the interstitial water volume and thus the volume fraction of isotropically diffusing protons; this necessarily reduces the total voxel anisotropic volume fraction [18]. Alternatively, more complex biophysical models of diffusion in WM like the neurite orientation dispersion and density imaging (NODDI) [19] model inherently compartmentalizes the isotropic and anisotropic volume fractions by modelling the diffusion signal as "free water" (isotropic; reflective of cerebrospinal fluid (CSF), interstitial fluid (ISF), edema, etc.), "intra-neurite", and "extra-neurite" tissues, as a sphere, stick, and tensor, respectively. One of the key derived metrics from NODDI is the orientation dispersion index (ODI), which quantifies the orientation coherence of neurites in each voxel and is analogous to the DTI-derived FA value [20], with the exception that

the diffusion signal fraction used to calculate this value is uncontaminated by more “isotropically diffusing” proton populations like those associated with edema.

Previous studies [21], [22], [23], [24], [25], [26], [27], [28], [29], [30] which also carried out analyses using DTI and NODDI in brain tumors, demonstrate the limitations of DTI in detecting WM in peritumoral regions and reported a reduction in FA values in edematous and tumoral regions. While these studies recognized both FA and ODI as distinguishing parameters of white matter tissue microstructure, the results of these studies must be interpreted with caution given the inclusion of heterogeneous pathological populations (e.g., glioma, brain metastases, and meningioma). For example, while both glioma and meningioma elicit peritumoral vasogenic edema, glioma displays dramatic tumor cell infiltration into neural tissue that compromises the microstructural integrity of white matter tracts [4], [5], [31]. Meningioma, however, typically occurs only within the meninges, which may displace brain tissue and drive increased hydrostatic pressure and downstream vasogenic edema, but otherwise leaves the brain unaffected [32]. By evaluating individuals with meningioma, it is possible to specifically isolate the effects of edema on WM tissue.

Thus, the purpose of this study was to assess the performance of the DTI-derived FA and NODDI-derived ODI in quantifying WM tracts in a controlled study in which regions of pure edema can be assumed (i.e., WM is uncontaminated by infiltrative tumor cells). We hypothesized that the use of the multi compartment model, NODDI, would enable a characterization of WM that is specific to the tissue (and unconfounded by the effects of edema). Furthermore, we hypothesized that ODI would yield higher accuracy in WM characterization than FA in patients with meningioma; specifically, we hypothesized that high FA and low ODI values would be observed in the healthy-appearing contralateral WM, whereas low FA and low

ODI values would be observed in regions containing edema-laden white matter. More specifically, neurite-specific indices of dispersion and orientation would allow for the characterization and visibility of WM pathways through pathological regions with high specificity. We also hypothesize seeing high fractional isotropic volume (FISO) values, as represented by the increased interstitial fluid volume due to edema.

2. Methods

2.1. Participant population

Six adults aged 62 to 77 years old bearing radiologically confirmed meningiomas were included in this study. Participant data were acquired and anonymized by the Mayo Clinic, Phoenix, Arizona and processed and analyzed at Arizona State University. All experimental procedures were approved by each institution's Institutional Review Board. Tumor locations included: participant 1 – frontal lobe, participant 2 – frontal lobe, participant 3 – left anterior limbic lobe, participant 4 – left occipital lobe, participant 5 – left occipital lobe, participant 6 – left frontal lobe (Figure 1 shows a panel of these participants' tumor locations (in a post contrast T1), edema regions (in a T2-FLAIR), and their associated FA, ODI and FISO maps).

2.2. Neuroimaging data acquisition

Imaging data were acquired on a 3T Siemens scanner using a 20-channel coil. Acquired imaging data include: (i) a three-dimensional (3D) axial T1-weighted magnetization prepared rapid acquisition gradient echo (MPRAGE) sequence, (ii) a 3D post-Gadolinium (Gd) T1-weighted MPRAGE sequence (TR/TE 1900/2.02 ms, 208 slices), (iii) a 3D T2-weighted fluid-attenuated inversion recovery (FLAIR) sequence (TR/TE 5000/389 ms, 192 slices) and (iv) multi-shell diffusion-weighted acquisitions with the following parameters: b-values (s/mm2) =

750 (12 directions), 1000 (18 directions), 1500 (24 directions), 2000 (30 directions) and 2500 (36 directions) (TR/TE 3664/95.6 ms, 185 slices). b-values ranging from 10 to 500 were also acquired in this dataset but are not informative to the models used herein and are thus neglected from here forward. All MR images were screened for neuropathology by a licensed neuroradiologist prior to analysis.

2.3. Diffusion neuroimaging pipeline

Only diffusion volumes with b-values of 0 and greater than 700 s/mm^2 were included to fit the NODDI model to the data but b-values= 0, 1000 s/mm^2 were used in the case of DTI. Data were corrected for noise (MRtrix) [33], field map distortion (Synb0) [34] and eddy currents (MRtrix and FSL) [35]. DTI (using FSL's DTIFIT toolbox) [36] and Watson-NODDI (using the NODDI MATLAB toolbox) [37] models were applied to preprocessed data to generate the zero-to-one-scaled FA and ODI maps, respectively; where high FA and low ODI reflect coherent directionality of WM tracts. All volumes were then co-registered to the pre-contrast T1-weighted volume. See supplemental Figures 1S and 2S for complete detailing of processing pipeline.

For each participant, the tumor region of interest (ROI) was identified and manually segmented using the post-contrast T1-weighted volume. The total edema ROI (including tumor and peritumoral edema) was identified and segmented based on the hyperintense signal of the T2-FLAIR. The extra-tumoral edema ROI was derived by subtracting the tumor segment from the total edema segment. As a control, healthy-appearing contralateral white matter tracts were identified by first flipping the extra-tumoral edema ROI over the midline and then manually adjusting the outline to include only white matter containing voxels as defined on the pre-contrast T1-weighted image. These ROIs were then overlaid on the FA and ODI maps and the location of each ROI was confirmed by a licensed neuroradiologist (see edema appearance in

these image volumes in in Figure 2). Additionally, to address the bias caused by CSF contamination in the ROI analysis, we implemented a tissue-weighted mean approach [38], [39]. Traditional methods average NODDI metrics like NDI and ODI across all voxels, which can lead to inaccuracies in areas with partial CSF volume. Our method uses tissue fraction (TF) maps, calculated as one minus the free water fraction (FWF), to adjust for this. By multiplying NDI and ODI by the TF, extracting their weighted means, and normalizing by the mean TF, we obtain more accurate estimates of the microstructure, effectively correcting for CSF contamination.

For tractography, we implemented "Fiber Assigned by Continuous Tracking" (FACT) (using MRtrix's tckgen package [40] and visualized using MI-Brain [41]). DTI-based FA maps, along with their respective primary direction vectors, were used as seed images for DTI-based tractography. A seed initiation threshold value of 0.60 and tract termination cutoff value of 0.50 was used (deduced from a histogram plot of FA values). For NODDI-based tractography, ODI maps were subtracted from one to satisfy thresholding assumptions intrinsic to the FACT software; namely that high values in the seed map indicate a high degree of directionality. These modified ODI maps, along with their respective primary direction vectors, were then used as seed images. A seed initiation threshold value of 0.88 and tract termination cutoff value of 0.84 was used (based on a previously defined correlation between FA and ODI values, [42] where an FA of 0.50 correlated to an ODI of approximately 0.16 and an FA of 0.60 correlated to an ODI of approximately 0.12 thus yielding ODI thresholds of 0.84 and 0.88 respectively after subtracting from one). Ventricle and white matter masks were created (using FSL). The ventricle mask was applied to exclude any streamlines in the region of ventricles, while the white matter mask restricted streamlines to the bounds of the white matter. A total of 10,000 streamlines were generated for both DTI-based and NODDI-based tractography.

Statistical analysis

Statistical analyses were completed with R version 4.2.2 (2022-10-31) [43]. A Shapiro-Wilks test was used to test the FA and ODI distributions for normality. t-tests were performed between WM FA values in edematous and contralateral non-edematous regions, and between ODI values for the same regions.

3. Results

Results also tabulated below in Table 1. The percentage differences in the FA values and the ODI values between edematous and non-edematous regions were calculated for each ROI (see Equations 1 and 2). All descriptive measures are summarized in Table 1.

Equation 1: $((\mathrm{FA}_{\mathrm{non-edematous}} - \mathrm{FA}_{\mathrm{edematous}})/\mathrm{FA}_{\mathrm{non-edematous}}) \times 100$

Equation 2: $((\mathrm{ODI}_{\mathrm{non-edematous}} - \mathrm{ODI}_{\mathrm{edematous}})/\mathrm{ODI}_{\mathrm{non-edematous}}) \times 100$

Table 1

Participant	Mean ± SD FA Ipsi	Mean ± SD FA Contra	Percent Difference ± SD FA	Mean ± SD ODI Ipsi	Mean ± SD ODI Contra	Percent Difference ± SD ODI
1	0.22±0.02	0.47±0.04	53.19±0.24	0.20±0.03	0.21±0.03	4.76±0.24
2	0.14± 0.04	0.46±0.01	69.57±0.32	0.19±0.07	0.18±0.07	-5.56±0.04
3	0.46±0.06	0.66±0.07	30.30±0.20	0.16±0.03	0.15±0.03	-6.67±0.004
4	0.25±0.02	0.57±0.08	56.14±0.32	0.14±0.03	0.13±0.03	-7.69±0.007
5	0.16±0.03	0.44±0.09	63.64±0.28	0.19±0.04	0.20±0.05	5.00±0.02
6	0.17± 0.02	0.51±0.08	66.67±0.34	0.20±0.03	0.19±0.05	-5.26±0.005

While FA values were high in contralateral white matter tracts, shown in Figure 3 (a), they were lower in edematous white matter tracts whereas the ODI values remained approximately in the same range for both regions as shown in Figure 3 (b). The results presented in Figure 3 (c) show the percent differences in the mean FA and ODI values present in the edematous and contralateral regions. There were no significant differences in the ODI values between edematous and non-edematous regions ($\beta = 0.0007$, 95% CI = [-0.03; 0.03], $p = 0.96$) but differences were significant in the FA values within these regions ($\beta = 0.29$, 95% CI = [0.16; 0.42], $p = 0.0008$).

Visualization of the distribution and participant relationship show participant WM ODI on the y-axis and FA on the x-axis for edematous and contralateral non-edematous side in Figure 3 (d) and demonstrates clearly how FA fails to delineate white matter in regions of edema (ipsilateral region) which can be seen through the considerable decrease in FA values in comparison to its readings in the normal appearing hemisphere (contralateral region). There is a dramatic shift in the histogram for FA values going from the edematous side to the contralateral healthy appearing side of the brain i.e., FA values are in the lower range (<0.5) for white matter in regions of edema while ODI values remain within comparable ranges for both sides of the brain.

Figure 4 (a) presents the NODDI-derived isotropic volume fraction (FISO) map and Figure 4 (b) shows the neurite density index (NDI) map for a participant with left hemisphere edema. The accompanying plots illustrate average voxel-wise FISO and NDI values in edematous regions compared to the contralateral healthy side. FISO values appear to capture intra-voxel levels of tumor-induced edema. This is supported by lower NDI values in edematous areas, which reflect the inverse relationship between neurite density and edema volume. Further

supporting this, T1-based volume analyses between edematous and contralateral sides revealed an average 54% increase in the number of voxels on the edematous side. This significant increase suggests the spread of interstitial fluid into white matter (WM), leading to volumetric expansion of the tissue.

Figures 5 displays representative DTI-FA- and NODDI-ODI-based tractography results. DTI-FA-based tractography fails to generate tracts in regions of edema, whereas NODDI-ODI-based tractography successfully characterizes tracts within the edematous regions.

4. Discussion

The purpose of this study was to determine if the NODDI-derived ODI parameter can better characterize WM tracts within regions of peri-tumoral edema as compared to standard-of-care DTI and FA. Consistent with our hypothesis, results indicated that ODI is insensitive to edema (i.e., ODI values in white matter tracts within edema remained comparable to those in non-edematous regions), whereas FA decreased substantially in edematous WM tracts across all participants. These findings suggest that ODI may have potential clinical utility as a robust measure of white matter anatomy in individuals with peritumoral edema.

Reduced FA values in edematous WM regions is likely due to the inherent inability of DTI, both from a data acquisition and calculation perspective, to separate more restricted from less restricted diffusion components and isotropic from anisotropic diffusion components within a single voxel. Multi-shell diffusion MRI, when analyzed with a biophysical model like NODDI, overcomes these limitations and is thus better able to define WM tracts through regions of edema. The ODI value serves as a more sensitive biomarker of neurite orientation where higher values indicate greater dispersion or variability in the orientations of the white matter fibers

whereas lower values suggest more alignment or coherence among the fibers in the examined region [44]. NODDI's calculation isolates the confounding isotropic volume fraction [45] (in the form of the FISO parameter) from the other parameter estimates and thus yields a better approximation of the orientation distribution index in voxels contaminated by the large isotropic volume fraction associated with edema [4], [5], [21].

While significant differences in diffusion metrics between edematous and non-edematous WM regions may reflect sensitivity to edema-related changes (such as increased free water), it may not be the best representation of WM microstructure characterization. This suggests potential confounding effects of edema on diffusion measurements, emphasizing the need for cautious interpretation in clinical assessments. While we assume that WM properties should be comparable between unaffected hemispheres, statistical significance alone does not guarantee reliable quantification, as it can be skewed by sample size. Furthermore, it is important to note that maybe ODI is insensitive to edema status, and specific to neurite compartment, as our results demonstrate that it remains consistent across edematous and non-edematous regions. We are not claiming statistical similarity but rather emphasizing that ODI provides a more stable and reliable measure of WM microstructure in the presence of edema, whereas FA is problematically sensitive to the effects of edema. Our findings support the hypothesis that ODI offers a more robust approach to characterizing WM in the presence of edema, which is crucial for pre-surgical planning.

As expected, regions with edema exhibited higher isotropic volume fraction (FISO), indicating that NODDI-derived parameters are sensitive to the expected effects of intra-voxel edema (increased interstitial fluid which thereby reduces intra-voxel neurite density). Indeed, this effect is also apparent on the macroscopic scale, where we see an apparent swelling of the white

matter tracts to such a degree that tissue is displaced into sulci (see Fig. 1, Participant 6 for example). This effect appears to propagate into the NODDI-ODI-based tractography results, in which we see successful visibility of tracts. Importantly, DTI-FA-based tractography fails to show any tracts in these regions.

Another observation made was lower neurite density index (NDI) values when compared to normal-appearing contralateral white matter. NDI is formulated as the intracellular volume fraction of tissue, after removing the isotropic component (FISO) i.e.,

$$\frac{V_{ic}}{V_{ic} + V_{ec}} = \frac{V_{ic}}{1 - V_{iso}}$$

where V_{ic}, V_{ec}, and V_{iso} represent volume fractions of intracellular, extracellular, and isotropic components, respectively. While regions of edema are expected to exhibit high FISO values due to the presence of isotropic free water, the concurrent reduction in NDI does not necessarily imply microstructural changes such as axonal degeneration or demyelination. This is particularly relevant in the context of meningiomas, which are non-invasive tumors known to displace white matter tracts rather than causing significant microstructural damage. The reduced NDI observed in edematous regions in our study may therefore reflect limitations of the NODDI model when applied to pathological conditions, rather than true alterations in tissue microstructure. These findings underscore the importance of cautious interpretation and highlight the need for histological validation to confirm whether microstructural changes occur in such contexts. Additionally, while high FISO values were anticipated, the reduced NDI values were an observational finding rather than a hypothesis-driven outcome, and we recognize this as a limitation of the study.

In the context of threshold-driven tractography, the study by Chong et al. (2021) [21], for example highlighted the use of NODDI to enhance tractography in regions affected by

peritumoral edema, demonstrating that NODDI-based tractography could visualize fiber tracts not detectable by standard DTI. They calibrated an optimal ODI threshold using the deterministic fiber tracking algorithm for the corticospinal tract (CST) in healthy subjects to then assess the differences between DTI and NODDI-derived tractography in a population of brain tumor subjects (a mixed population of high and low grade tumors like gliomas and meningiomas). In contrast to tumor-infiltrated regions, where tumor cells complicate assessments, our study specifically examines WM regions in subjects with non-invading meningioma tumors wherein WM is unaffected by tumor cells; for this reason, we are able to isolate the effects of edema from other likely confounds like tumor infiltration and demyelination. By incorporating these controls and systematically comparing tractography outcomes across DTI and NODDI, we demonstrate NODDI's superior performance in viewing tract integrity in the presence of edema.

It is important to note that NODDI may overestimate FISO in white matter regions due to its assumption of a single T2 relaxation time constant across all tissue compartments. However, our study operates within the constraints of a clinical dataset that does not include the necessary data to measure multi-exponential T2 relaxation times. While this suggests that NODDI may overestimate ODI and NDI values, no evidence of such overestimations was observed in this study. Thus our a priori hypothesis was that ODI values would remain consistent across both edematous and non-edematous white matter regions, with no expectation of change. Therefore, we found no basis to conclude that NDI or ODI values were significantly affected by this potential issue. Our findings support the hypothesis that ODI is not measurably affected by the presence of edema. Additionally, the tissue-weighted means method (used here) [38] also addresses CSF contamination, unlike traditional approaches that average NODDI metrics across all ROI voxels. It uses NODDI's tissue fraction metrics to adjust for varying CSF levels among

voxels, leveraging the model's explicit representation of tissue and CSF compartments which enables a more accurate capture of microstructural information across the ROI. Implementing such a correction could improve the accuracy of NODDI-derived metrics in regions affected by edema, leading to more reliable microstructural characterization in clinical applications.

In this study, we focused on using the NODDI model to differentiate between the isotropic (containing the edema fraction) and anisotropic (white matter) diffusion components in meningioma cases [18], [19], [32], [46]. In this case, we are assessing the value of a biophysical model in WM characterization in a controlled trial where meningioma induces only edema (i.e., no WM disruption or tumor invasion is expected). This approach contrasts with previous studies that have compared NODDI and DTI across heterogeneous populations involving various tumor types, where the surrounding tissue environment can be more complex (often involving destruction of WM tracts) [22], [24], [25], [27]. Here we demonstrate NODDI's ability to specifically separate tumor-driven vasogenic edema from WM microstructure. While signal-based methods like free water elimination-DTI (FW-DTI) [47] also address free-water contamination, our interests are towards deriving metrics from biophysical models like NODDI in the context of all brain tumor, including glioma, in which microstructural changes to WM are expected. Furthermore, the successful illustration of tractography using NODDI metrics serves to showcase its potential application in clinical scenarios where accurate mapping of white matter pathways is crucial for planning surgical approach to tumor resection. Ongoing work includes comparative analyses with other methods such as FW-DTI and CSD (constrained spherical deconvolution) [48] to extend the use of multi-shell diffusion MRI and advanced diffusion modeling in complex contexts like invasive glioma.

Historic challenges to deploying these methods include collection of multi-shell datasets which required increased acquisition times; however, the emergence of multiband, parallel imaging, and compressed sensing acquisition schemes has dramatically reduced acquisition times to the point where dMRI datasets that satisfy the NODDI model can now be acquired in approximately five minutes [29]. Importantly, multi-shell datasets open the door to other models but don't preclude DTI and its use in standard clinical procedures. While in this work we have ensured the presence of only edema in imaged tissue via selective inclusion of only meningioma-bearing participants, future studies will need to focus on the more complex cases of invasive tumors like high grade gliomas. The study of invasive primary brain tumors in this context would also greatly benefit from complementary rodent studies in which dMRI results can be directly validated against histologic and assay studies; studies which are ongoing in this laboratory. Finally, future work will involve expansion into other biophysical models of diffusion in brain tissue, including variations on the Standard Model [49] like the Soma And Neurite Density Imaging (SANDI) model [50] and the Neurite Exchange Imaging (NEXI) [51] in both clinical and preclinical settings.

5. Conclusions

In this proof-of-concept study, we assessed the performance of DTI and NODDI in detecting WM in edematous and non-edematous brain regions. Our results indicated that the ODI detected WM in edema (also supported through tractography results), whereas FA did not. We also report that NODDI's FISO parameter seems to uniquely capture the water fraction associated with edema. These findings suggest that multi-shell diffusion MRI, when coupled with advanced biophysical models like NODDI, provide a far more robust insight into pathologic tissue as compared to standard of care DTI. As an example, presurgical planning may benefit

from implementing NODDI-based methods, rather than standard-of-care DTI. Future work will further evaluate the clinical utility of using NODDI-derived measures to localize critical WM tracts prior to tumoral resection.

Acknowledgments

This work was supported by NIH grant U01CA220378 (L.S.H); NIH grant U01CA250481 (L.S.H.); NIH grant R01CA264992 (L.S.H.); NIH grant R01CA221938 (L.S.H.); NIH grant R21NS082609 (LSH.); K01 EB032898; the Mayo Clinic & ASU Alliance for Health Care— Collaborative Research Seed Grant Program; the ASU-Mayo Summer Residency program (SCB, LSH) and the Arizona Biomedical Research Center (SCB).

Conflicts of Interest

Potential conflicts: Precision Oncology Insights (co-founders: L.S.H.); Imaging Biometrics (medical advisory board L.S.H.); IQ-AI Ownership Interest (L.S.H.) Imaging Biometrics Financial Interest (L.S.H.).

References

[1] Z. Chen et al., “Corticospinal tract modeling for neurosurgical planning by tracking through regions of peritumoral edema and crossing fibers using two-tensor unscented Kalman filter tractography,” Int. J. Comput. Assist. Radiol. Surg., vol. 11, no. 8, pp. 1475–1486, Aug. 2016, doi: 10.1007/s11548-015-1344-5.

[2] S. Gong et al., “Free water modeling of peritumoral edema using multi-fiber tractography: Application to tracking the arcuate fasciculus for neurosurgical planning,” PLOS ONE, vol. 13, no. 5, p. e0197056, May 2018, doi: 10.1371/journal.pone.0197056.

[3] E. C. A. Kaal and C. J. Vecht, “The management of brain edema in brain tumors:,” Curr. Opin. Oncol., vol. 16, no. 6, pp. 593–600, Nov. 2004, doi: 10.1097/01.cco.0000142076.52721.b3.

[4] J. Lecoeur, E. Caruyer, M. Elliott, S. Brem, L. Macyszyn, and R. Verma, “Addressing the Challenge of Edema in Fiber Tracking”.

[5] R. Liao et al., “Performance of unscented Kalman filter tractography in edema: Analysis of the two-tensor model,” NeuroImage Clin., vol. 15, pp. 819–831, Jan. 2017, doi: 10.1016/j.nicl.2017.06.027.

[6] H. Zhang et al., “Differences Between Generalized Q-Sampling Imaging and Diffusion Tensor Imaging in the Preoperative Visualization of the Nerve Fiber Tracts Within Peritumoral Edema in Brain,” Neurosurgery, Sep. 2013, doi: 10.1227/NEU.0000000000000146.

[7] S. E. Maier, Y. Sun, and R. V. Mulkern, “Diffusion imaging of brain tumors,” NMR Biomed., vol. 23, no. 7, pp. 849–864, Aug. 2010, doi: 10.1002/nbm.1544.

[8] F. Yamasaki et al., “Apparent Diffusion Coefficient of Human Brain Tumors at MR Imaging1,” Radiology, Jun. 2005, doi: 10.1148/radiol.2353031338.

[9] C. Hogea, C. Davatzikos, and G. Biros, “Modeling Glioma Growth and Mass Effect in 3D MR Images of the Brain,” in Medical Image Computing and Computer-Assisted Intervention – MICCAI 2007, N. Ayache, S. Ourselin, and A. Maeder, Eds., Berlin, Heidelberg: Springer, 2007, pp. 642–650. doi: 10.1007/978-3-540-75757-3_78.

[10] P. J. Basser and C. Pierpaoli, “Microstructural and physiological features of tissues elucidated by quantitative-diffusion-tensor MRI,” J. Magn. Reson., vol. 213, no. 2, pp. 560–570, Dec. 2011, doi: 10.1016/j.jmr.2011.09.022.

[11] S. Coelho, J. M. Pozo, S. N. Jespersen, and A. F. Frangi, “Optimal Experimental Design for Biophysical Modelling in Multidimensional Diffusion MRI,” in Medical Image Computing and Computer Assisted Intervention – MICCAI 2019, D. Shen, T. Liu, T. M. Peters, L. H. Staib, C. Essert, S. Zhou, P.-T. Yap, and A. Khan, Eds., in Lecture Notes in Computer Science. Cham: Springer International Publishing, 2019, pp. 617–625. doi: 10.1007/978-3-030-32248-9_69.

[12] I. O. Jelescu, M. Palombo, F. Bagnato, and K. G. Schilling, “Challenges for biophysical modeling of microstructure,” J. Neurosci. Methods, vol. 344, p. 108861, Oct. 2020, doi: 10.1016/j.jneumeth.2020.108861.

[13] H. Johansen-Berg and T. Behrens, Diffusion MRI: From Quantitative Measurement to In vivo Neuroanatomy: Second Edition. Elsevier, 2013. Accessed: Jan. 26, 2024. [Online]. Available: https://ora.ox.ac.uk/objects/uuid:15e45ac3-dab3-4f0f-a980-e4e56e1682ad

[14] B. Lampinen et al., “Searching for the neurite density with diffusion MRI: Challenges for biophysical modeling,” Hum. Brain Mapp., vol. 40, no. 8, pp. 2529–2545, 2019, doi: 10.1002/hbm.24542.

[15] D. S. Novikov, E. Fieremans, S. N. Jespersen, and V. G. Kiselev, “Quantifying brain microstructure with diffusion MRI: Theory and parameter estimation,” NMR Biomed., vol. 32, no. 4, Apr. 2019, doi: 10.1002/nbm.3998.

[16] A. Tropine et al., “Contribution of Diffusion Tensor Imaging to Delineation of Gliomas and Glioblastomas,” J Magn Reson Imaging, vol. 20, pp. 905–912, 2004, doi: 10.1002/jmri.20217.

[17] P. S. Yen, B. T. Teo, C. H. Chiu, S. C. Chen, T. L. Chiu, and C. F. Su, “White matter tract involvement in brain tumors: a diffusion tensor imaging analysis,” Surg. Neurol., vol. 72, no. 5, pp. 464–469, Nov. 2009, doi: 10.1016/J.SURNEU.2009.05.008.
[18] A. Qiu et al., “NODDI-DTI: Estimating Neurite Orientation and Dispersion Parameters from a Diffusion Tensor in Healthy White Matter,” Front. Neurosci. Wwwfrontiersinorg, vol. 11, 2017, doi: 10.3389/fnins.2017.00720.
[19] H. Zhang, T. Schneider, C. A. Wheeler-Kingshott, and D. C. Alexander, “NODDI: Practical in vivo neurite orientation dispersion and density imaging of the human brain,” NeuroImage, vol. 61, no. 4, pp. 1000–1016, 2012, doi: https://doi.org/10.1016/j.neuroimage.2012.03.072.
[20] N. Wang et al., “Neurite orientation dispersion and density imaging of mouse brain microstructure,” Brain Struct. Funct., vol. 224, no. 5, pp. 1797–1813, Jun. 2019, doi: 10.1007/s00429-019-01877-x.
[21] S. T. Chong et al., “Exploring Peritumoral Neural Tracts by Using Neurite Orientation Dispersion and Density Imaging,” Front. Neurosci., vol. 15, Sep. 2021, doi: 10.3389/fnins.2021.702353.
[22] Y. Kadota et al., “Differentiation between glioblastoma and solitary brain metastasis using neurite orientation dispersion and density imaging,” J. Neuroradiol., vol. 47, no. 3, pp. 197–202, May 2020, doi: 10.1016/J.NEURAD.2018.10.005.
[23] S. H. Li et al., “Application of Neurite Orientation Dispersion and Density Imaging in Assessing Glioma Grades and Cellular Proliferation,” World Neurosurg., vol. 131, pp. e247–e254, Nov. 2019, doi: 10.1016/j.wneu.2019.07.121.
[24] J. Mao et al., “Differentiation between high-grade gliomas and solitary brain metastases: a comparison of five diffusion-weighted MRI models,” BMC Med. Imaging, vol. 20, no. 1, Dec. 2020, doi: 10.1186/s12880-020-00524-w.
[25] S. Masjoodi, H. Hashemi, M. A. Oghabian, and G. Sharifi, “Differentiation of Edematous, Tumoral and Normal Areas of Brain Using Diffusion Tensor and Neurite Orientation Dispersion and Density Imaging,” J. Biomed. Phys. Eng., vol. 8, no. 3, pp. 251–260, Sep. 2018.
[26] I. I. Maximov, A. S. Tonoyan, and I. N. Pronin, “Differentiation of glioma malignancy grade using diffusion MRI,” Phys. Med., vol. 40, pp. 24–32, Aug. 2017, doi: 10.1016/j.ejmp.2017.07.002.
[27] Y. Okita et al., “Neurite orientation dispersion and density imaging and diffusion tensor imaging to facilitate distinction between infiltrating tumors and edemas in glioblastoma,” Magn. Reson. Imaging, vol. 100, pp. 18–25, Jul. 2023, doi: 10.1016/j.mri.2023.03.001.
[28] V. Pieri et al., “Along-tract statistics of neurite orientation dispersion and density imaging diffusion metrics to enhance MR tractography quantitative analysis in healthy controls and in patients with brain tumors,” Hum. Brain Mapp., vol. 42, no. 5, pp. 1268–1286, Apr. 2021, doi: 10.1002/hbm.25291.
[29] Q. Wen et al., “Clinically feasible NODDI characterization of glioma using multiband EPI at 7 T,” NeuroImage Clin., vol. 9, pp. 291–299, 2015, doi: 10.1016/j.nicl.2015.08.017.
[30] U. Würtemberger et al., “Differentiation of Perilesional Edema in Glioblastomas and Brain Metastases: Comparison of Diffusion Tensor Imaging, Neurite Orientation Dispersion and Density Imaging and Diffusion Microstructure Imaging,” Cancers, vol. 15, no. 1, Jan. 2023, doi: 10.3390/cancers15010129.
[31] H. J. SCHERER, M.D., “STRUCTURAL DEVELOPMENT IN GLIOMAS,” Am. J. CANCER, vol. E XXXIV, no. 3, Nov. 1938.
[32] Cheng-Hong Toh, Alex M-C Wong, Kuo-Chen Wei, Shu-Hang Ng, Ho-Fai Wong, and Yung-Liang Wan, “Peritumoral Brain Edema in Meningiomas□: Correlation of Radiologic and Pathologic Features,” 2011, doi: 10.3340/jkns.2011.49.1.26.
[33] J.-D. Tournier et al., “MRtrix3: A fast, flexible and open software framework for medical image processing and visualisation,” NeuroImage, vol. 202, p. 116137, Nov. 2019, doi: 10.1016/j.neuroimage.2019.116137.
[34] K. G. Schilling et al., “Synthesized b0 for diffusion distortion correction (Synb0-DisCo),” Magn. Reson. Imaging, vol. 64, pp. 62–70, Dec. 2019, doi: 10.1016/J.MRI.2019.05.008.

[35] M. Jenkinson, C. F. Beckmann, T. E. J. Behrens, M. W. Woolrich, and S. M. Smith, “FSL,” NeuroImage, vol. 62, no. 2, pp. 782–790, Aug. 2012, doi: 10.1016/j.neuroimage.2011.09.015.
[36] “FSL Diffusion Toolbox Practical.” Accessed: Jan. 26, 2024. [Online]. Available: https://fsl.fmrib.ox.ac.uk/fslcourse/2019_Beijing/lectures/FDT/fdt1.html
[37] “Microstructure Imaging Group | Download NODDI matlab toolbox.” Accessed: Jan. 25, 2024. [Online]. Available: http://mig.cs.ucl.ac.uk/index.php?n=Download.NODDI
[38] C. Parker, “Not all voxels are created equal: reducing estimation bias in regional NODDI metrics using tissue-weighted means,” Chris Parker - Research Blog. Accessed: Nov. 14, 2024. [Online]. Available: https://csparker.github.io/research/2021/11/16/Tissue-weighted-mean.html
[39] T. Veale, tdveale/TissueWeightedMean. (Mar. 21, 2024). Shell. Accessed: Nov. 14, 2024. [Online]. Available: https://github.com/tdveale/TissueWeightedMean
[40] “tckgen — MRtrix 3.0 documentation.” Accessed: Oct. 26, 2023. [Online]. Available: https://mrtrix.readthedocs.io/en/dev/reference/commands/tckgen.html
[41] imeka/mi-brain. (Jul. 06, 2024). Imeka. Accessed: Aug. 02, 2024. [Online]. Available: https://github.com/imeka/mi-brain
[42] H. Fukutomi et al., “Diffusion Tensor Model links to Neurite Orientation Dispersion and Density Imaging at high b-value in Cerebral Cortical Gray Matter,” Sci. Rep., vol. 9, no. 1, p. 12246, Aug. 2019, doi: 10.1038/s41598-019-48671-7.
[43] “R: The R Project for Statistical Computing.” Accessed: Jan. 25, 2024. [Online]. Available: https://www.r-project.org/
[44] F. Grussu et al., “Neurite dispersion: a new marker of multiple sclerosis spinal cord pathology?,” Ann. Clin. Transl. Neurol., vol. 4, no. 9, pp. 663–679, 2017, doi: 10.1002/acn3.445.
[45] A. Faiyaz, M. Doyley, G. Schifitto, J. Zhong, and M. N. Uddin, “Single-shell NODDI using dictionary-learner-estimated isotropic volume fraction,” NMR Biomed., vol. 35, no. 2, p. e4628, 2022, doi: 10.1002/nbm.4628.
[46] GCS Ramsay Santé pour l’Enseignement et la Recherche, “Evaluation of the Contribution of NODDI Protocol Tractography in Brain Tumor Surgery,” clinicaltrials.gov, Clinical trial registration NCT05669326, Dec. 2022. Accessed: Dec. 31, 2023. [Online]. Available: https://clinicaltrials.gov/study/NCT05669326
[47] S. S. Panesar, K. Abhinav, F.-C. Yeh, T. Jacquesson, M. Collins, and J. Fernandez-Miranda, “Tractography for Surgical Neuro-Oncology Planning: Towards a Gold Standard,” Neurotherapeutics, vol. 16, no. 1, p. 36, Dec. 2018, doi: 10.1007/s13311-018-00697-x.
[48] F.-C. Yeh, A. Irimia, D. C. de A. Bastos, and A. J. Golby, “Tractography methods and findings in brain tumors and traumatic brain injury,” NeuroImage, vol. 245, p. 118651, Dec. 2021, doi: 10.1016/j.neuroimage.2021.118651.
[49] S. Coelho et al., “Reproducibility of the Standard Model of diffusion in white matter on clinical MRI systems,” Feb. 04, 2022, arXiv: arXiv:2202.02399. Accessed: Feb. 06, 2024. [Online]. Available: http://arxiv.org/abs/2202.02399
[50] M. Palombo et al., “SANDI: A compartment-based model for non-invasive apparent soma and neurite imaging by diffusion MRI,” NeuroImage, vol. 215, p. 116835, Jul. 2020, doi: 10.1016/J.NEUROIMAGE.2020.116835.
[51] I. O. Jelescu, A. de Skowronski, F. Geffroy, M. Palombo, and D. S. Novikov, “Neurite Exchange Imaging (NEXI): A minimal model of diffusion in gray matter with inter-compartment water exchange,” NeuroImage, vol. 256, p. 119277, Aug. 2022, doi: 10.1016/J.NEUROIMAGE.2022.119277.

Figures

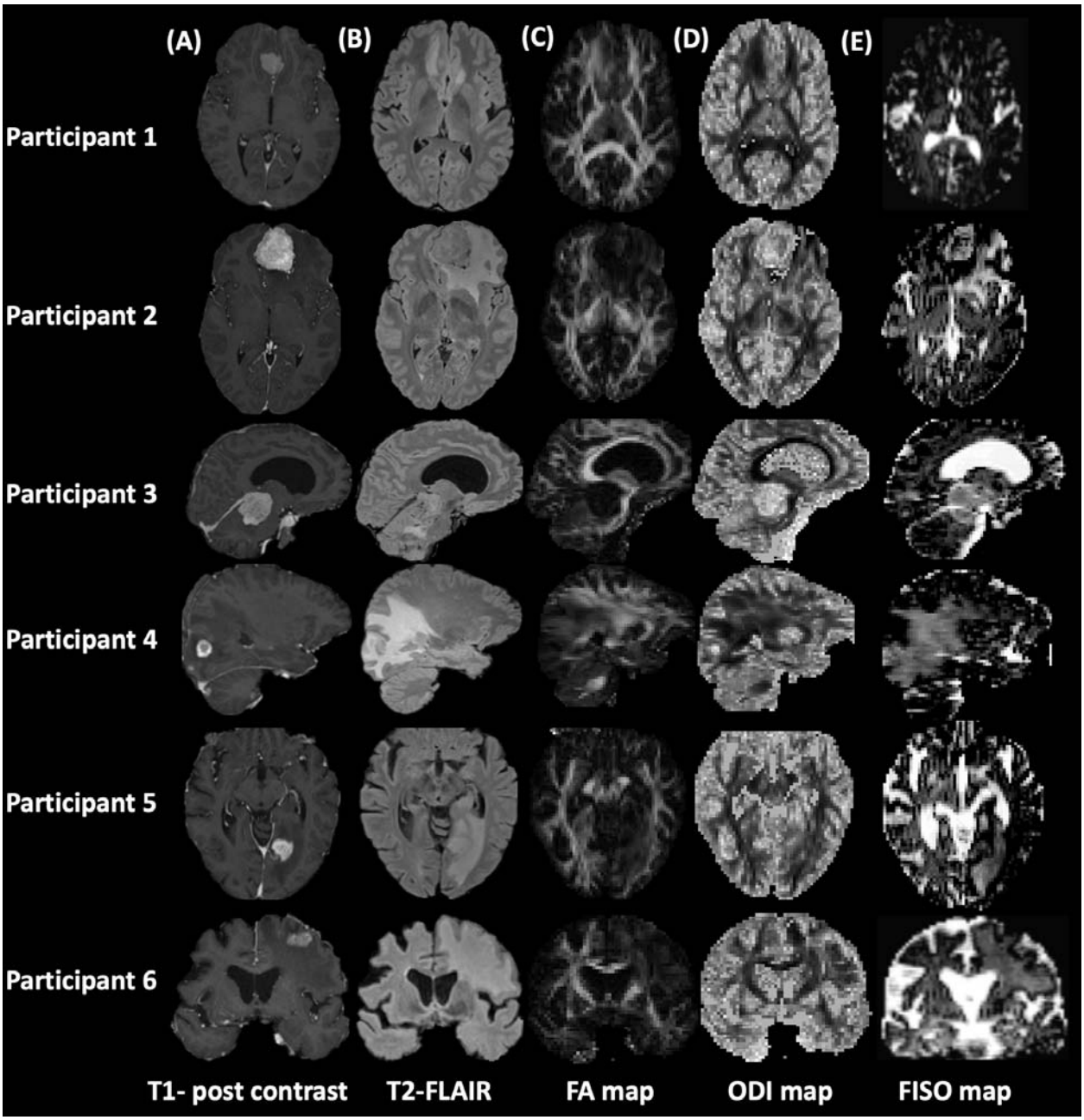

Figure 1. Representative post-contrast T1-weighted images (A), T2-weighted FLAIR images (B), FA maps (C), ODI maps (D) and Isotropic volume fraction (FISO) maps (E) are shown. Post-contrast T1-weighted images best reflect tumor location and T2-weighted FLAIR images best reflect tumor plus edema location. FA (where WM is typically represented by a brighter signal

intensity) fails to robustly characterize WM tracts though regions of edema (seen as hyperintense signal traced in T2-FLAIR images) whereas ODI (where WM is represented by a darker signal intensity) retains WM structure irrespective of edema presence. Representative image plane was chosen on a per-patient basis to best reflect the lesion.

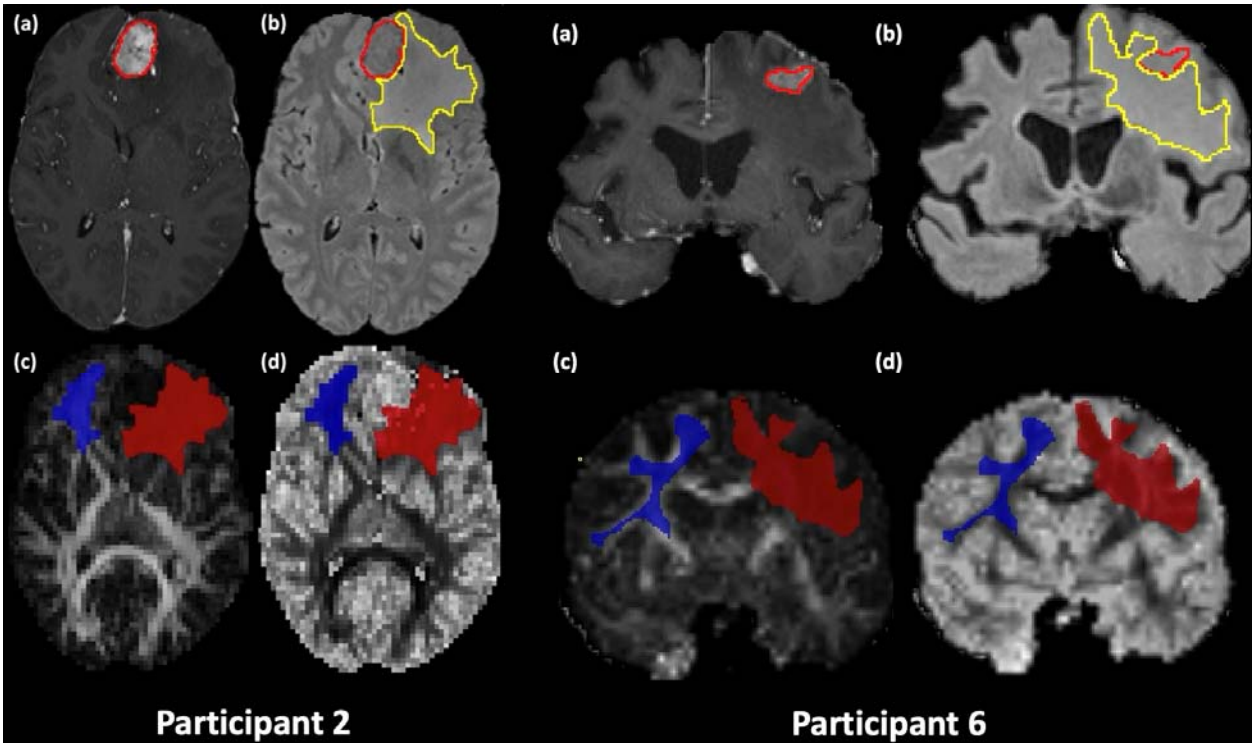

Figure 2. Example ROI placements on T1-post Gd and T2-FLAIR images and FA and ODI maps. (a) T1- post Gd image with tumor contour (red), (b) T2- FLAIR image with tumor (red) and edema (yellow) contours, (c) FA and (d) ODI maps with edema (in red) and the contralateral region (in blue) highlighted. For each participant, the tumor contour was identified and segmented using the T1-weighed post-contrast volume and was then overlaid the T2-weighted FLAIR image; then the peritumoral edematous contour was identified and segmented based on the hyperintense signal in the T2-FLAIR. The region highlighting extra-tumoral edema was then derived by subtracting the two segmentations (i.e., FLAIR region of interest minus the post-contrast T1-weighted region of interest). As a control, healthy-appearing contralateral white

matter tracts were identified by first flipping the edema ROI over the midline and then manually adjusting the outline to include only white matter containing voxels. A T1-weighted image was used to verify locations of contralateral WM tract ROIs. These ROIs were then overlaid on the FA and ODI maps and the location of each ROI was confirmed by a licensed neuroradiologist. Participants' MRIs were then co-registered to their T1-weighted image.

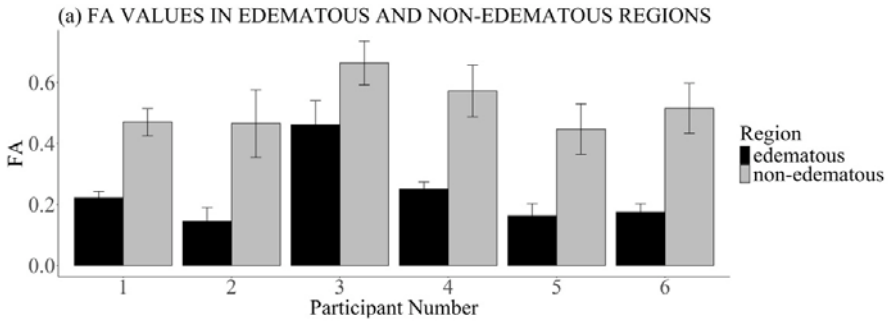
(a) FA VALUES IN EDEMATOUS AND NON-EDEMATOUS REGIONS
FA
0.0
0.2
0.4
0.6
1
2
3
4
5
6
Participant Number
Region
edematous
non-edematous

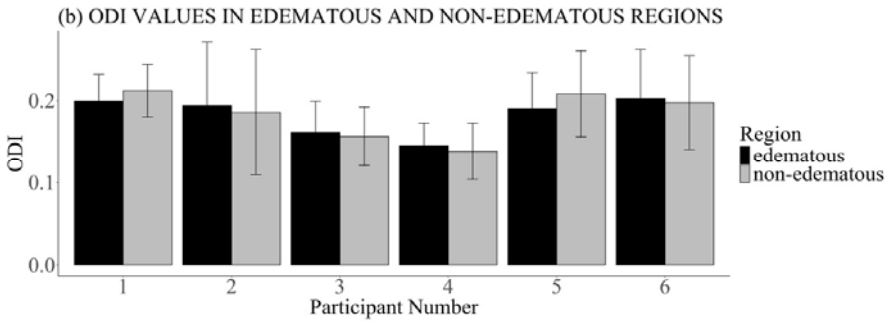
(b) ODI VALUES IN EDEMATOUS AND NON-EDEMATOUS REGIONS
ODI
0.0
0.1
0.2
1
2
3
4
5
6
Participant Number
Region
edematous
non-edematous

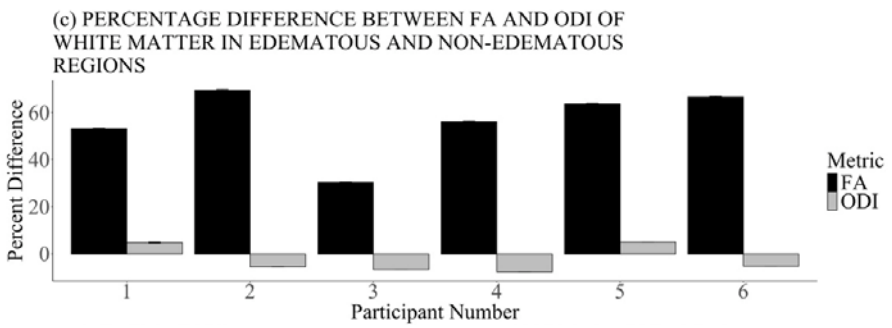
(c) PERCENTAGE DIFFERENCE BETWEEN FA AND ODI OF WHITE MATTER IN EDEMATOUS AND NON-EDEMATOUS REGIONS
Percent Difference
0
20
40
60
1
2
3
4
5
6
Participant Number
Metric
FA
ODI

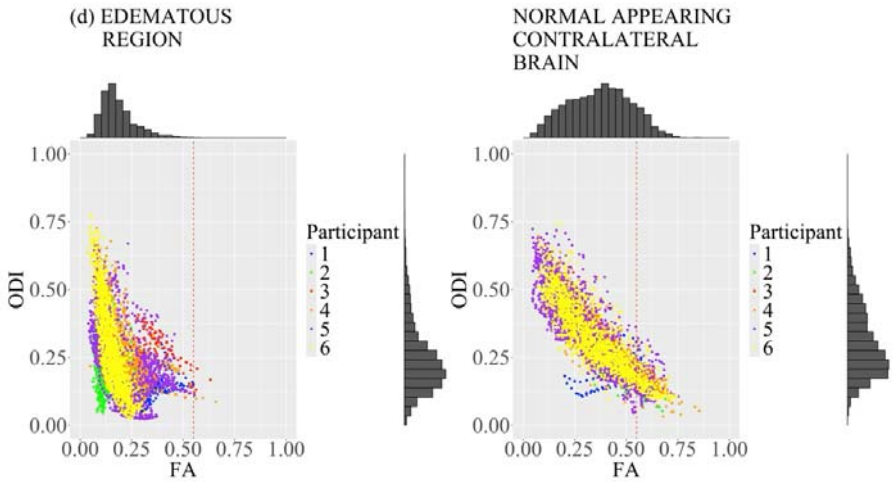
(d) EDEMATOUS REGION
NORMAL APPEARING CONTRALATERAL BRAIN
ODI
0.00
0.25
0.50
0.75
1.00
FA
Participant
1
2
3
4
5
6

Figure 3. (a) FA values in edematous and non-edematous regions. (b) ODI values between white matter regions of interest in edematous and non-edematous regions. (c) Bar graph illustrating the percentage difference between FA and ODI of white matter tracts in edematous and non-edematous regions. (d) Histogram and scatter plot of FA and ODI values for all participants. Participant WM ODI is on the y-axis and FA is on the x-axis for edematous (left panel) and comparable normal-appearing contralateral WM regions (right panel) regions. Each data point in the scatter plot represents a voxel in the region of interest with colors corresponding to participant number. Higher FA and lower ODI values are indicative of white matter presence in a voxel. The left panel illustrates that FA values are significantly reduced for white matter in regions of edema as compared to the contralateral regions. The range of ODI values appears to remain consistent in both edematous and contralateral regions thus indicating successful white matter voxel detection in both regions. Thus, we see a clear shift in the range of FA values, going from <0.5 for white matter in regions of edema to the expected higher range of 0.5-0.75 in the normal appearing contralateral side of the brain. The ODI values are observed to be within the same range regardless of the presence of edema thus suggesting more robust white matter detectability.

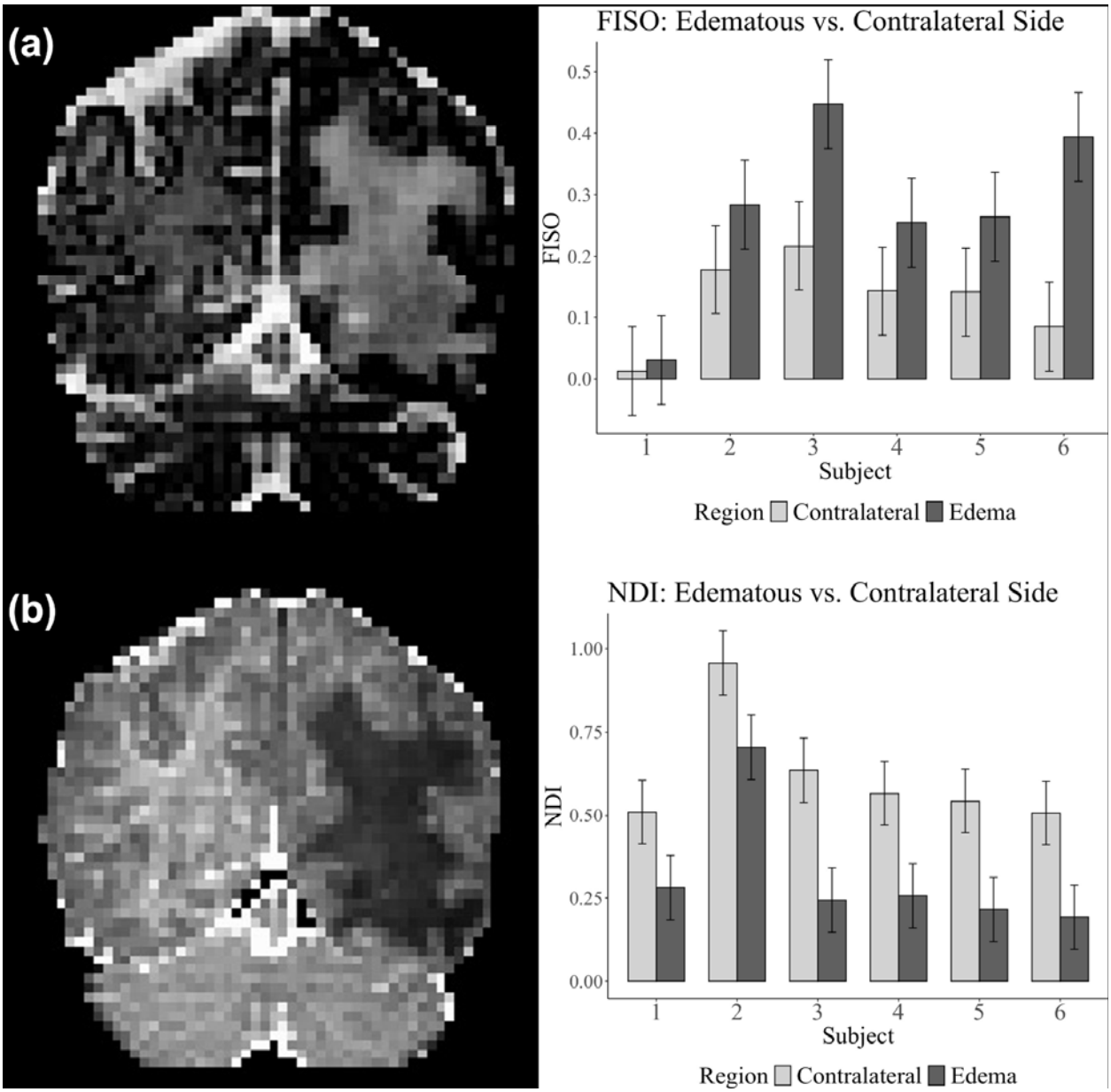

Figure 4. (a) Representative NODDI-derived isotropic volume fraction (FISO) and (b) neurite density index (NDI) maps for a participant with meningioma-induced edema. Plots represent voxel-wise (a) FISO and (b) NDI values in regions of edema versus regions in the contralateral healthy-appearing side of the brain. FISO values were found to be higher in the edematous region, likely due to an increased volume of tumor-induced edema. In contrast, NDI values were found to be lower in edematous regions.

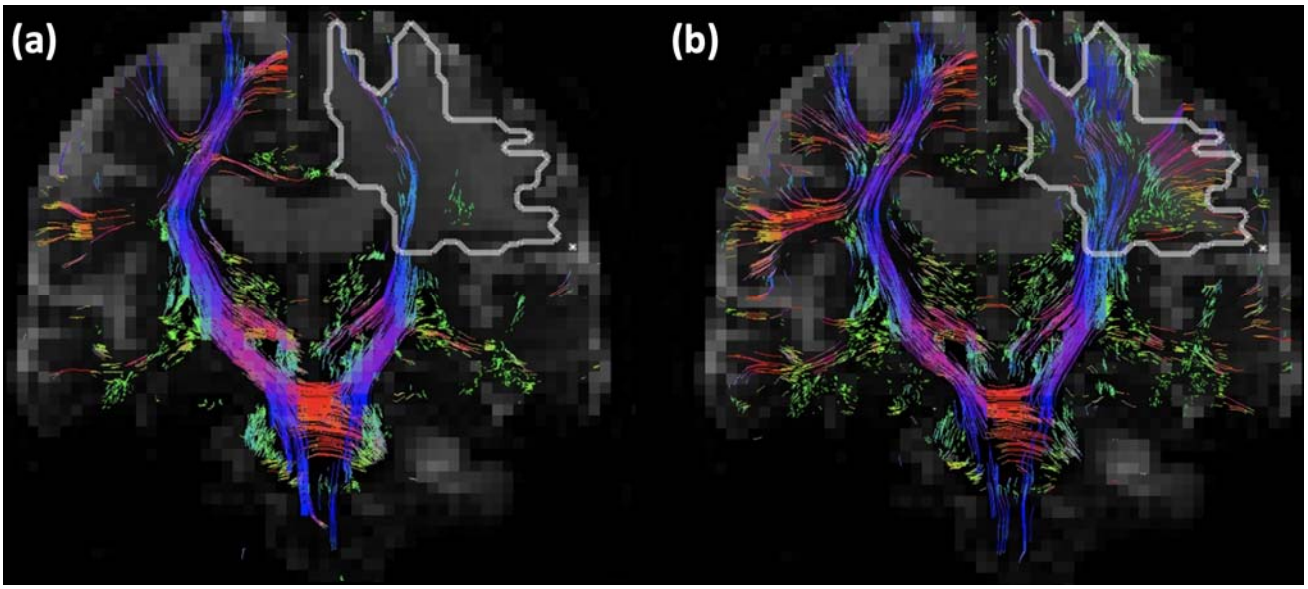

Figure 5. A representative coronal plane from whole-brain tractography results obtained using deterministic (a) DTI-based (left) and (b) NODDI-based tracking (right). NODDI-ODI successfully track white matter in the region of edema (demarcated by the white outline) where DTI-FA fails.

Supplemental Figures

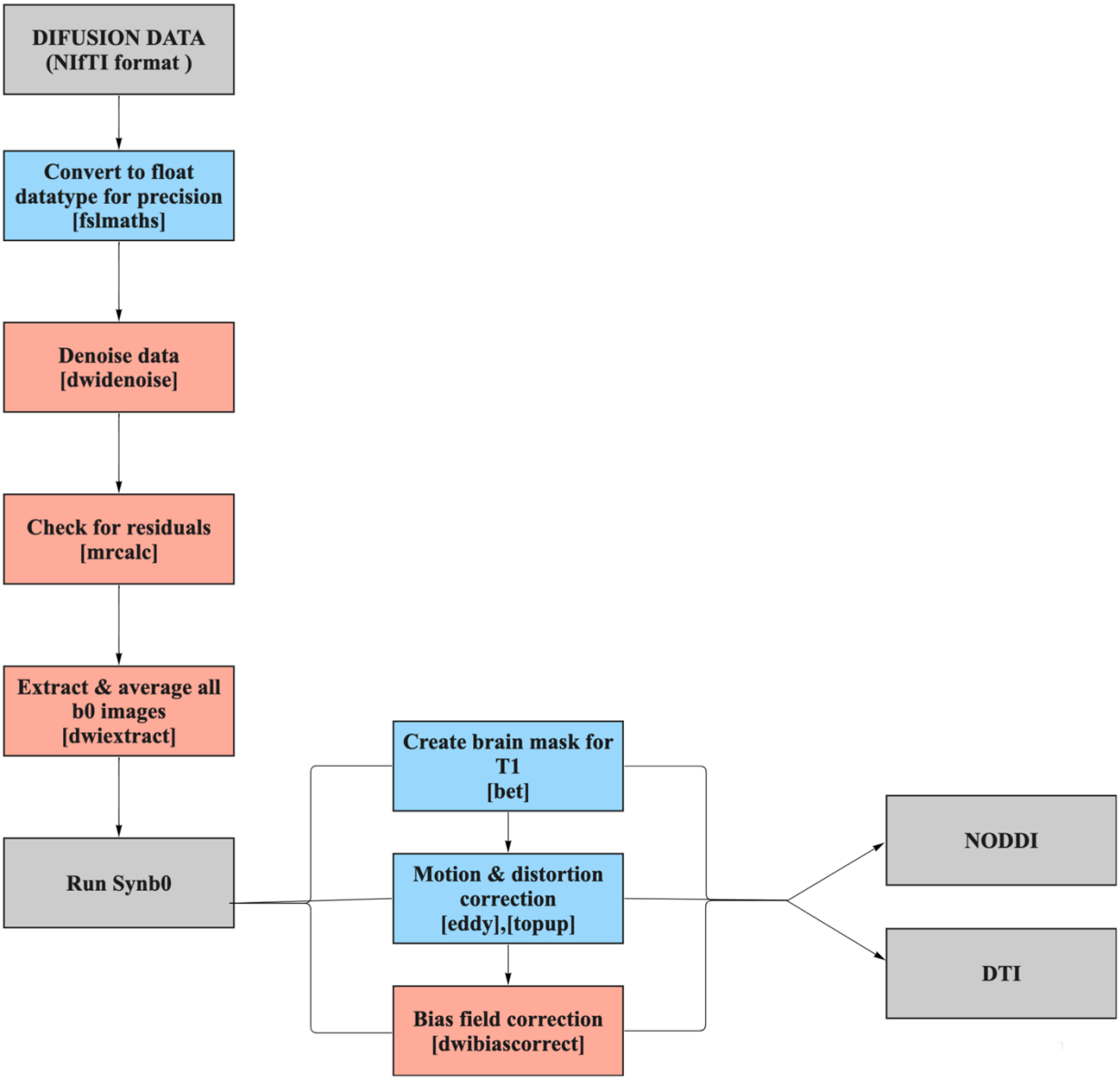

Figure 1S. The image pre-processing workflow illustrated above uses a combination of tools accessible through pre-packaged softwares like FSL (blue boxes) and MRtrix (red boxes) to-convert raw diffusion data to a float datatype for greater precision, denoise the data, extract and average b0 image volumes, run the syn-b0 algorithm to generate a synthetic b0 image that facilitates the subsequent application of topup and eddy algorithms that help correct for artifacts

and distortions, followed by the implementation of DTI (FSL) and NODDI (Matlab) diffusion models. These codes and commands were executed using a bash script.

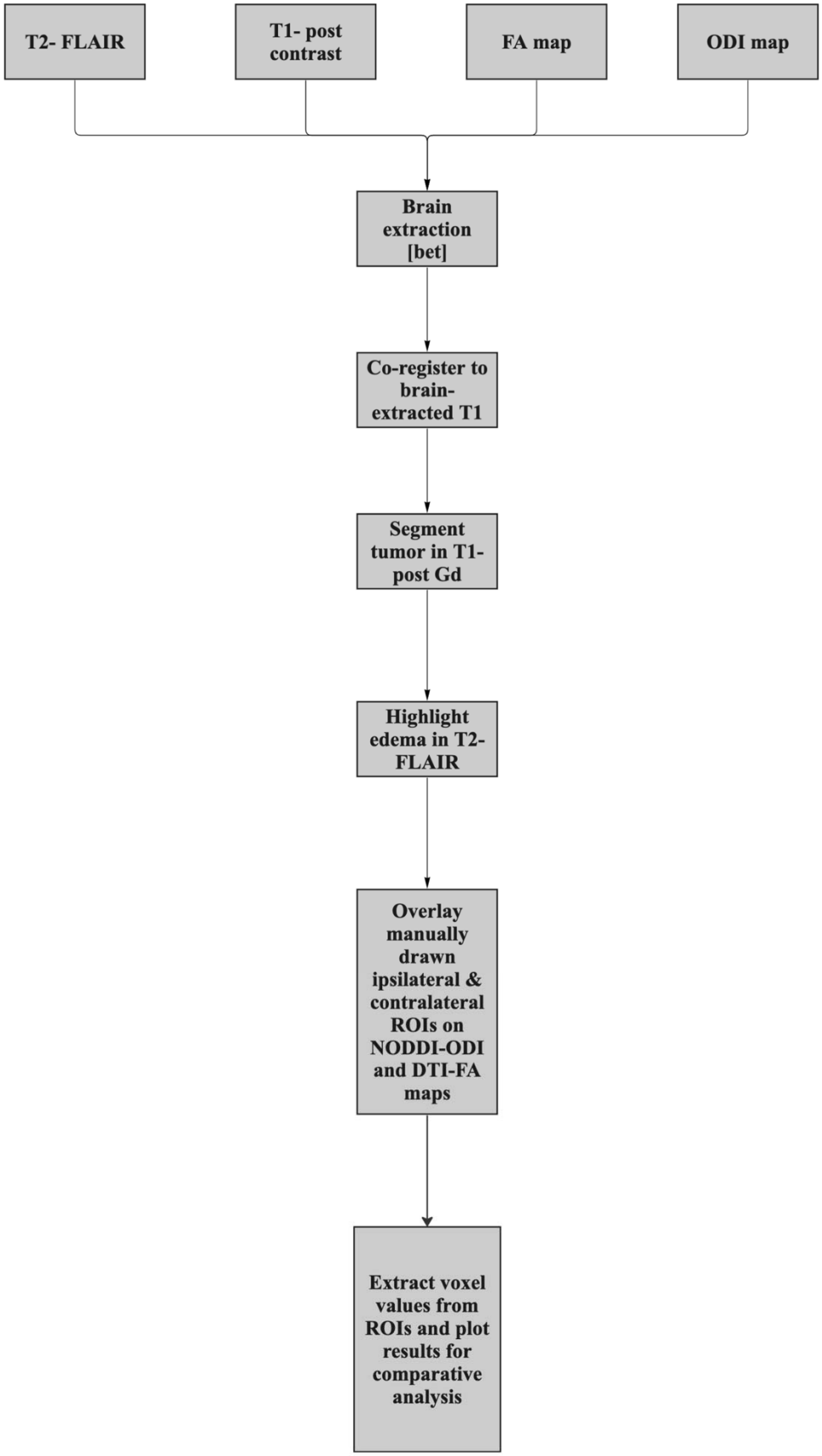
T2- FLAIR
T1- post contrast
FA map
ODI map
Brain extraction [bet]
Co-register to brain-extracted T1
Segment tumor in T1-post Gd
Highlight edema in T2-FLAIR
Overlay manually drawn ipsilateral & contralateral ROIs on NODDI-ODI and DTI-FA maps
Extract voxel values from ROIs and plot results for comparative analysis

Figure 2S. The post-processing pipeline illustrated above explains the steps involved, specific to this analysis wherein required images (T1-post contrast, T2-FLAIR, FA map and ODI map) underwent brain-extraction and then co-registration to the structural pre-contrast T1-weighted image. The region of interest (ROI) defining the location of tumor was segmented using a T1-post contrast image and the ROI defining the extent of peri-tumoral edema was segmented using a T2-FLAIR. The ROI hence defining the region of extra-tumoral edema was obtained by subtracting the aforementioned ROIs. These manually drawn ROIs were then flipped along the axis to obtain a contralateral ROI in the normal-appearing side of the brain and then manually adjusted according to the white matter tract appearance in the T1 image. The ROIs were overlaid on the NODDI-derived ODI and DTI-derived FA maps to extract voxel-wise metrics from these regions to ultimately undergo a statistical analysis.